13TH CANADIAN MASONRY SYMPOSIUM
HALIFAX, CANADA
JUNE 4TH – JUNE 7TH 2017

EFFECTS OF FLANGED BOUNDARY ELEMENTS ON THE RESPONSE OF SLENDER REINFORCED MASONRY SHEAR WALLS: AN EXPERIMENTAL STUDY

Robazza, B.R.[1]; Brzev, S. [2]; Yang, T.Y.[3]; Elwood, K.J.[4]; Anderson, D.L.[5] and McEwen, W.[6]

ABSTRACT

Reinforced masonry shear walls (RMSWs) have been demonstrated to possess adequate ductility and energy dissipation characteristics for seismic design applications. However, slender RMSWs, characterized by high height-to-thickness (h/t) ratios, may be vulnerable to out-of-plane instability under in-plane seismic loading. Out-of-plane instability is a failure mechanism that affects RMSW end-zone regions subjected to cycles of tensile strain, followed by compressive strain during load reversal. This failure mechanism has the potential to cause unexpected and rapid strength degradation or collapse, if not considered in design. The Canadian masonry design standard, CSA S304-14, prescribes h/t limits for the seismic design of RMSWs to prevent out-of-plane instability, however, no experimental testing verifies these limits. Moreover, the h/t limits are independent of the cross-sectional shape of the RMSW, despite the wall response being significantly influenced by this parameter. At a given drift demand, T-shaped RMSWs, i.e. rectangular RMSWs with flanged boundary elements at one end-zone, tend to produce higher strains at the end-zone without flanged boundary elements as compared to the end-zones of rectangularly-shaped RMSWs. This may increase the risk of out-of-plane instability affecting T-shaped RMSWs. This paper describes the findings of an experimental test-series aimed to identify the effects of flanged boundary elements on the response of slender RMSWs subjected to in-plane seismic loading. The paper presents a summary of qualitative observations and test results, as well as a discussion on the key differences in response characteristics of slender RMSWs with T-shaped compared to those of rectangular cross-sections.

KEYWORDS: *reinforced masonry, out-of-plane response, in-plane loading*

[1] Corresponding author, Ph.D. Candidate, Dept. of Civil Eng., Univ. of British Columbia (UBC) 2329 W Mall, Vancouver, BC, V6T 1Z4, Canada, E-mail : brook.robazza@civil.ubc.ca, Phone: 778-840-3773
[2] Former Faculty, Dept. of Civil Eng., British Columbia Institute of Technology, 3700 Willingdon Ave, Burnaby, BC, V5G 3H2, Canada, E-mail: svetlana.brzev@gmail.com
[3] Professor, Dept. of Civil Eng., UBC, 2329 W Mall, Vancouver, BC, V6T 1Z4, Canada, yang@civil.ubc.ca
[4] Professor, Dept. of Civil Eng., Univ. of Auckland, Auckland 1142, PB 92019, NZ, k.elwood@auckland.ac.nz
[5] Emeritus Professor, Dept. of Civil Eng., UBC, 2329 W Mall, Vancouver, BC, V6T 1Z4, Canada, dla@civil.ubc.ca
[6] Former Exec. Director, MIBC, 3636 E 4th Ave., Vancouver, BC, V5M 1M3, Canada, info@masonrybc.org

INTRODUCTION

In Western Canada, reinforced masonry shear walls (RMSWs) often form the lateral force resisting system of buildings such as warehouses or pump stations, which consist of tall slender walls with low levels of axial loading. During a seismic event, the end-zones of these walls are subjected to cyclic loading that is characterized by excursions of high tensile strain followed by smaller excursions of compressive strain; the magnitude disparity between these strains being dependent on the reinforcement details and the width of the extreme compression fiber. For walls lightly loaded in axial compression, increasing ductility levels may induce critical magnitudes of tensile strain at one end-zone, potentially precipitating out-of-plane instability of the end-zone upon directional reversal of the load. This failure mechanism occurs in several forms, ranging from localized instability of the vertical reinforcement at the wall toes, to brittle collapse of an entire wall end-zone. The various classes of out-of-plane instability may be categorized as follows (see Figure 1):

- Class A: localized buckling of vertical reinforcement at the wall toe.
- Class B: unstable out-of-plane displacements of the wall end-zone following the initiation of face shell spalling and toe-crushing.
- Class C: unstable out-of-plane displacements of the wall end-zone prior to the initiation of face shell spalling.

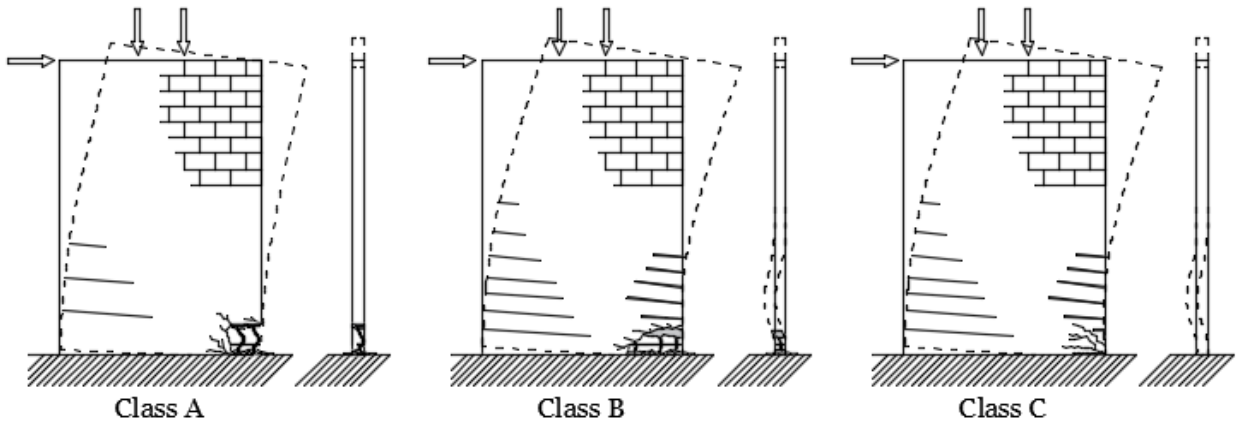

Figure 1. Out-of-plane instability mechanism classes in RMSWs

The ultimate capacity of a RMSW typically coincides with the initiation of face shell spalling, thus Class C out-of-plane instability mechanisms are of the most concern as it has the potential to cause unexpected failure of the wall. Class A and B instability mechanisms are less dangerous as they occur only after loading has exceeded the design levels. The Canadian masonry design standard, CSA S304-14, prescribes slenderness restrictions in the form height-to-thickness (h/t) ratio limits to account for Class C instability, but these potentially simplistic limits have not been experimentally verified. Moreover, h/t limits fail to account for numerous important parameters that affect the potential for out-of-plane instability in RMSWs, including the presence of flanged boundary elements at only one end-zone of a rectangularly-shaped wall.

T-shaped walls are common around doorways and other openings in warehouse and pump station buildings. Compared to rectangular walls, T-shaped walls tend to experience higher curvature demands when lateral loads are acting toward the flanged end-zone. As such, tensile strains at the web end-zone may become very large prior to face shell spalling at the flanged end-zone, creating a higher vulnerability toward Class C instability. This theoretical vulnerability to instability has however not been verified in the few experimental studies that involved slender T-shaped RMSWs:

- Shedid et al. (2008) conducted quasi-static reversed-cyclic tests on a series of rectangular, end-confined, and T-shaped RMSWs with h/t's ranging from 13.7 to 18.9, but none of the T-shaped RMWS experienced any type of out-of-plane instability.
- He and Priestly (1992), conducted both quasi-static and dynamic reversed-cyclic tests on 9 T-shaped specimens with h/t's of 25.6, but observed only a single Class B instability in one of the quasi-statically tested specimens.

This paper describes an experimental test series that further expands the experimental database of T-shaped RMSWs and investigates their susceptibility to out-of-plane instability. The test series forms a part of an ongoing experimental program that has examined the effects of height-to-thickness (h/t) ratio, height-to-length (h/L) aspect ratio, vertical and horizontal content and distribution, and the level of applied axial stress, on the out-of-plane response of rectangularly-shaped RMSWs (Robazza et al. 2015a; 2015b). The objective of the current test series was to investigate the effects of flanged boundary elements on the response of RMSWs subjected to in-plane lateral loading, with special attention given to the out-of-plane behaviour. The paper provides a summary of the specimen responses and the key findings of the tests.

EXPERIMENTAL PROGRAM

To experimentally study the effects of flanged boundary elements on the in-plane and out-of-plane response of RMSWs, two of the three slender full-scale RMSW specimens had T-shaped cross-sections and the other had a rectangular cross-section (see Table 1). The three specimens are identical in design except for the presence of boundary elements and the symmetry of the loading scheme. The tests were conducted using reversed-cyclic loading applied near the top of each specimen, which continued until the lateral load carrying capacity reached 80% of its peak.

Table 1: Experimental Test Matrix

ID	Wall Design Parameters								Loading Protocol Type	Sliding Restraint Device
	h (mm)	t (mm)	L (mm)	ρ_v (%)	ρ_h (%)	h/t --	h/L --	Plan Shape --		
W6	4000	190	2600	0.27	0.26	21.1	1.5	T-Section	Asymmetric	No
W7	4000	190	2600	0.27	0.26	21.1	1.5	T-Section	Symmetric	Yes
W8	4000	190	2600	0.24	0.26	21.1	1.5	Rectangular	Symmetric	Yes

Wall Selection Criteria

Walls with higher h/t ratios are more susceptible to out-of-plane instability and thus the h/t ratio of the specimens was selected to be the maximum permissible by the testing facility; 21.1, thus exceeding the CSA S304-14 limits. Out-of-plane instability can only occur in walls exhibiting flexure-dominated behaviour, and is more likely to occur in walls with longer plastic hinge heights. Considering that a flexure-dominated response requires a minimum h/L of 1.5, and that plastic hinge height increases with wall length (Paulay and Priestley 1992), an intermediate h/L of 1.5 was selected for the test specimens. For the T-shaped W6 and W7 specimens, the flanges consisted of 200x200 mm boundary elements on both faces of one end zone, as shown in Figure . These flanged boundary elements increased the effective width of the extreme compression fiber, thus reducing the compressive stress at the flanged end-zone and enabling higher levels of tensile strain at the web end-zone to be reached prior to toe-crushing or face shell spalling initiating. Another measure to increase the probability of out-of-plane instability was through strain manipulation; using an asymmetric loading protocol in the case of specimen W6. By incrementally increasing displacement amplitudes of load cycles directed toward the flanged end-zone, while maintaining constant displacement amplitudes for loading toward the web end-zone, it was possible to develop high tensile strains at the web end-zone while maintaining low compressive strains during load reversal.

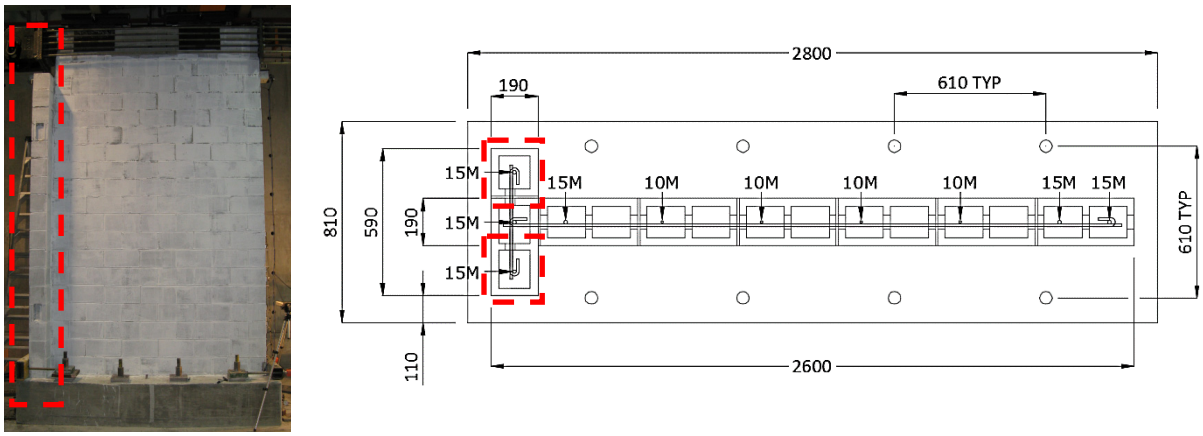

a) **b)**

Figure 2: Flanged boundary elements of specimens W6 and W7: a) elevation and b) plan.

Large sliding shear displacements that preclude the development of out-of-plane instability (Robazza et al. 2015a) were controlled by restraint devices installed at both wall toes of specimens W7 and W8 (see Figure 3). These devices were not post-tensioned, permitting a small amount of sliding to prevent excessive confinement of the wall toe.

The masonry units consisted of standard Canadian concrete masonry units (390 mm long x 190 mm high) with two hollow cores and constructed in 50% running bond using commercially available Type S mortar in accordance with CSA S304-14. The masonry was reinforced

horizontally and vertically with steel reinforcing bars detailed in accordance with the CSA S304-14 requirements for Ductile Shear Walls. The quantity and distribution of the horizontal reinforcement was sufficient to prevent diagonal tension shear failure in the specimens and consisted of 10M bars placed in bond beam units that were terminated with 180° hooks at the ends, resulting in a horizontal reinforcement ratio (ρ_h) of 0.26%.

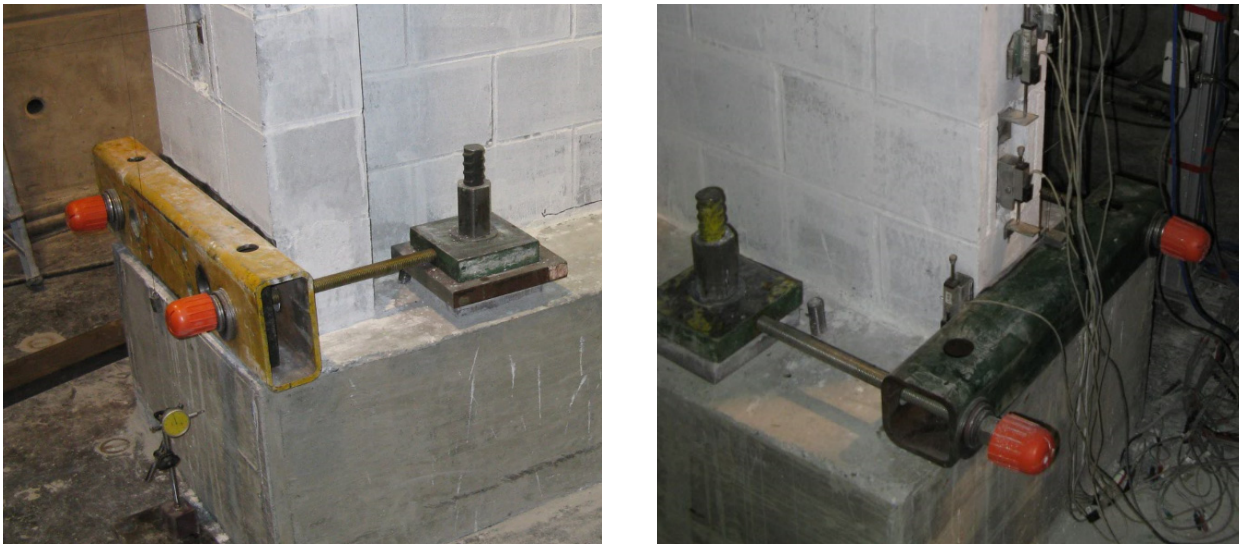

a) **b)**

Figure 3: Sliding restraints at a flanged end-zone a), and at a web end-zone b).

Additional L-shaped horizontal reinforcing bars were provided at the vertical web-flange interface of specimens W6 and W7 to prevent an interface shear failure occurring at that location. The vertical reinforcement consisted of 10M bars distributed along the wall length and 15M bars set in the end-zones and flanged boundary elements, resulting in average vertical reinforcement ratios (ρ_v) of 0.27%, for specimens W6 and W7, and 0.24% for specimen W8. The vertical reinforcing bars were continuous over the wall height and were fully developed in reinforced concrete footings that were anchored to the rigid reaction floor of the UBC testing facility. Additional vertical dowel reinforcing bars were placed at the top five courses of each specimen to prevent sliding shear failure developing near the end plates that transmitted the actuator loads to the specimen. The specimens were fully grouted with a commercially available coarse grout mix, which met the requirements of CSA S304-14. “Clean-out” ports were placed at the base of the specimens at 400 mm spacing to ensure proper grout consolidation at the bottom courses. The grouting of all specimens was performed in two lifts to reduce possibly air voids.

Material testing was provided in accordance with the pertinent Canadian Standards Association (CSA) standards. Masonry unit testing was performed per CSA A165-04 (Canadian Standards Association 2004a) and found an average net compressive strength of 27.4 MPa based on at least five masonry units per wall specimen. Mortar and grout testing was performed in accordance with the CSA A179-04 (Canadian Standards Association 2004b) and found an compressive

strength of 12.6 MPa based on an average of 9 standard-50 mm mortar cubes per wall specimen. The average grout compressive strength was 35.7 MPa, based on the results of 10 tests per wall specimen. Each grout sample was 100 mm in diameter, 200 mm-high and cast in a non-absorptive mould. The masonry compressive strength, f'_m, was determined per CSA S304-14 by performing compressive strength tests on two-unit-high grouted masonry prisms. Five two-unit high prism tests for each wall specimen determined an average compressive strength of 26.4 MPa. The horizontal and vertical reinforcing bars were Grade 400 steel with a nominal yield strength of 400 MPa. A minimum of 10 tensile tests were conducted for each wall specimen using 10M and 15M reinforcing bar coupons. The tests were performed in compliance with CSA G301.18-M92-R2002 (Canadian Standards Association 2004c) and found an average uniaxial yield strength of 503 MPa, corresponding to an average yield strain of approximately 0.003.

2.2 Test Setup and Loading Protocol

A custom-designed test setup was developed for the experimental program using a horizontal actuator with a load capacity of ±1000 kN and a ±343 mm stroke. The actuator was supported by a rigid reaction wall and connected to the load-transfer apparatus via pin-connections, as illustrated in Figure 4. The load-transfer apparatus consisted of steel load application plates that secured the top of the specimens at each end using 10 high-strength post-tensioning rods. The RMSW specimens represented walls in single-storey structures with low levels of axial precompression and therefore no vertical loading was applied to the specimens. A set of custom-designed out-of-plane restraints prevented out-of-plane displacements at the top of the specimens during the testing. These restraints created near-pinned support conditions in the transverse wall and a roller connection in the longitudinal direction.

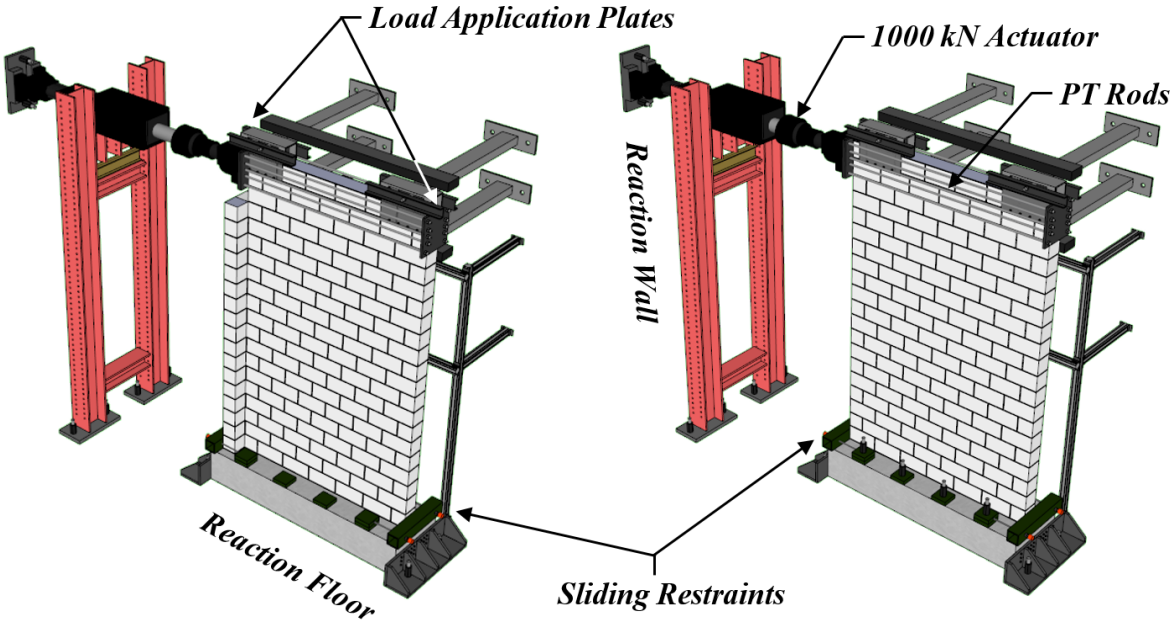

Figure 4: Test setup for specimens: a) W6 and W7, and b) W8.

Figure 5 shows the displacement-controlled loading protocol executed for specimen W6, while those of specimens W7 and W8 are shown in Figure 6. For the asymmetric loading protocol of specimen W6, the displacement-controlled loading cycles, hereafter referred to as "drift cycles," increased at increments ranging from 0.5 to 2.0 times Δ_y during loading in the direction of the flanged end-zone, but remained constant during loading in the direction of the web end-zone once the increments reached $2.0\Delta_y$ (0.37% drift); Δ_y is the drift corresponding to the onset of first-yielding of the outermost longitudinal reinforcing bars at the web end-zone of W6. This value was found to be 0.18% drift, or 7 mm lateral displacement between the point of load application and the wall base.

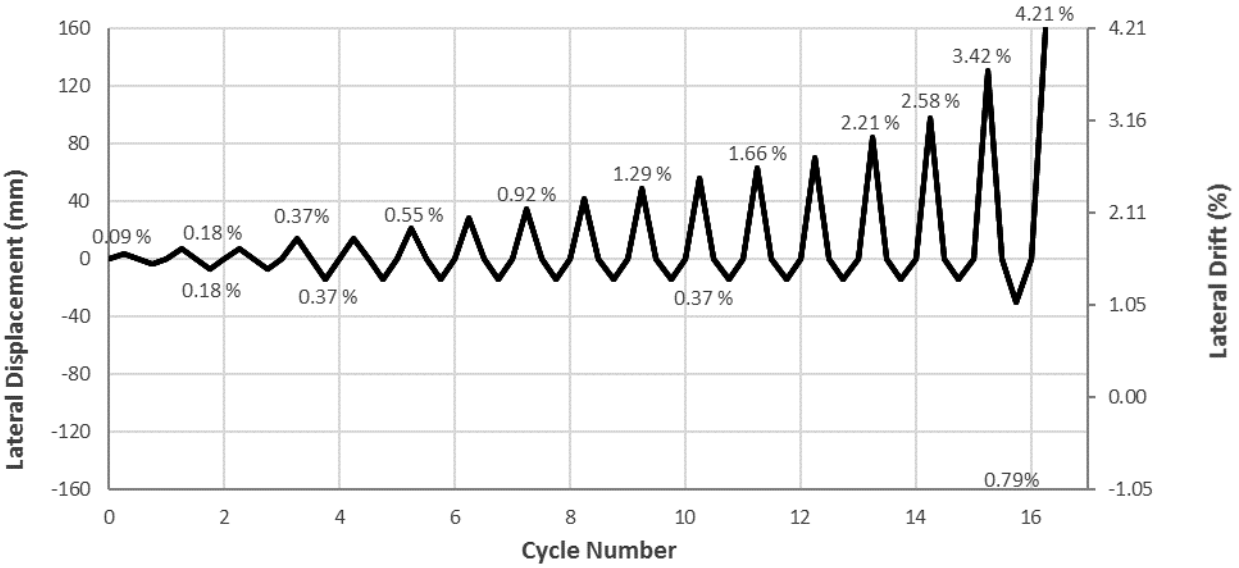

Figure 5: Displacement-controlled loading protocol for the tests on specimen W6.

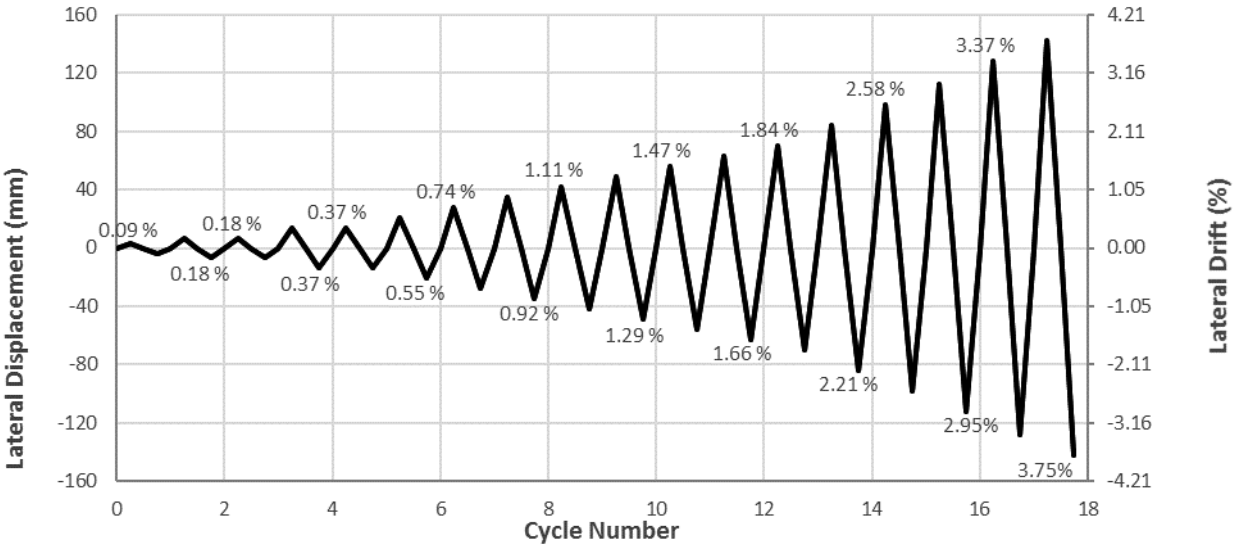

Figure 6: Displacement-controlled loading protocol for the tests on specimens W7 and W8.

EXPERIMENTAL RESULTS

Figure 7 provides a visual comparison of the lateral load-displacement behaviour of the specimens, with positive lateral displacement defined as longitudinal translation toward the web end zone. Contrasting the response of specimens W6 and W7 yields the effects of loading protocol symmetry on the in-plane response of the walls; besides the evident difference in the positive direction, the negative direction responses of the specimens were comparable in terms of peak strength, initial stiffness, and reloading stiffness. The response of specimen W6 was however somewhat less ductile than specimen W7 after it attained its maximum lateral load-carrying capacity. This may be attributed in part to the difference in the magnitude of sliding displacement between the specimens because the restraints installed on specimen W7 acted to significantly reduce sliding at most ductility levels compared to the freely sliding W6.

The energy dissipation, i.e. the area under the load-displacement curve, in the top-left quadrant of the lateral load-displacement hystereses was 84% greater for specimen W6 compared to specimen W7. Due to the asymmetric loading protocol, the levels of axial compressive stress at the web end zone of specimen W6 were much lower, inhibiting toe-crushing and face shell spalling. This allowed the plastic tensile strains in the vertical reinforcement to accumulate and remain laterally-supported by the surrounding masonry throughout compression excursions, preventing bar buckling and the associated soft response to vertical compression.

A comparison of the T-shaped specimen W7 and the rectangularly-shaped W8 reveals some important effects caused by flanged boundary elements as well. The most apparent difference is that specimen W7 exhibited a 59% higher peak strength during positive direction loading. This can be explained by the significantly higher volume of vertical reinforcement at the flanged end zone contributing to the negative direction strength of the wall. Despite the higher ultimate strength, specimen W7 experienced positive direction strength degradation that was 190% more rapid than specimen W8; the final residual strength was also 7% lower than specimen W8. This is primarily due to the compression-controlled nature of the flexural resistance to loading toward the web end zone and the associated heavy face shell spalling and toe crushing that follows attainment of ultimate capacity. The peak strength due to negative direction loading was also higher for specimen W7 compared to specimen W8 due to its additional flange area creating a greater moment arm for flexural resistance; the wall strength was however tension-controlled in this direction and thus the additional strength was limited to 10% of specimen W8's capacity.

The negative direction strength degradation was 77% more rapid and the reloading stiffness was 55% lower on average for specimen W8 compared to specimen W7. This may be attributed to the flanged end zone of specimen W7 maintaining its out-of-plane alignment throughout the test, offering restraint and stiffness not provided to specimen W8; the out-of-plane displacements experienced throughout the test by specimen W8 at both end zones throughout the testing appeared to cause more rapid toe-crushing and face shell spalling compared to specimen W7.

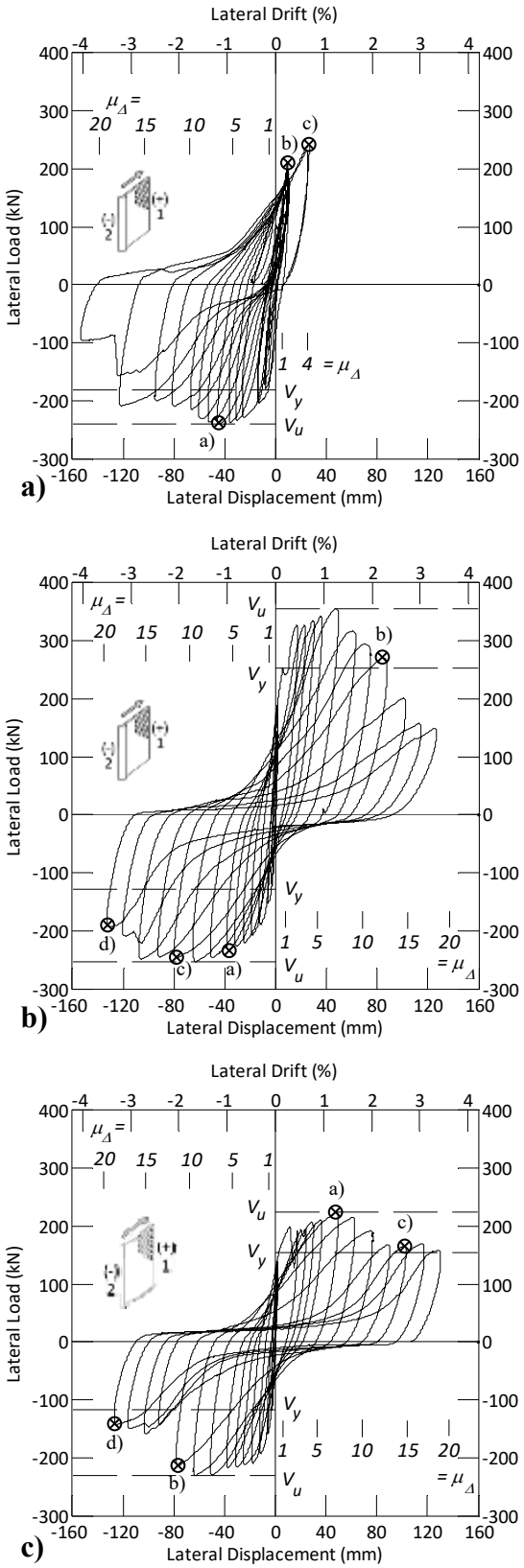

Figure 7: Lateral load-displacement curves: a) W6, b) W7, and c) W8.

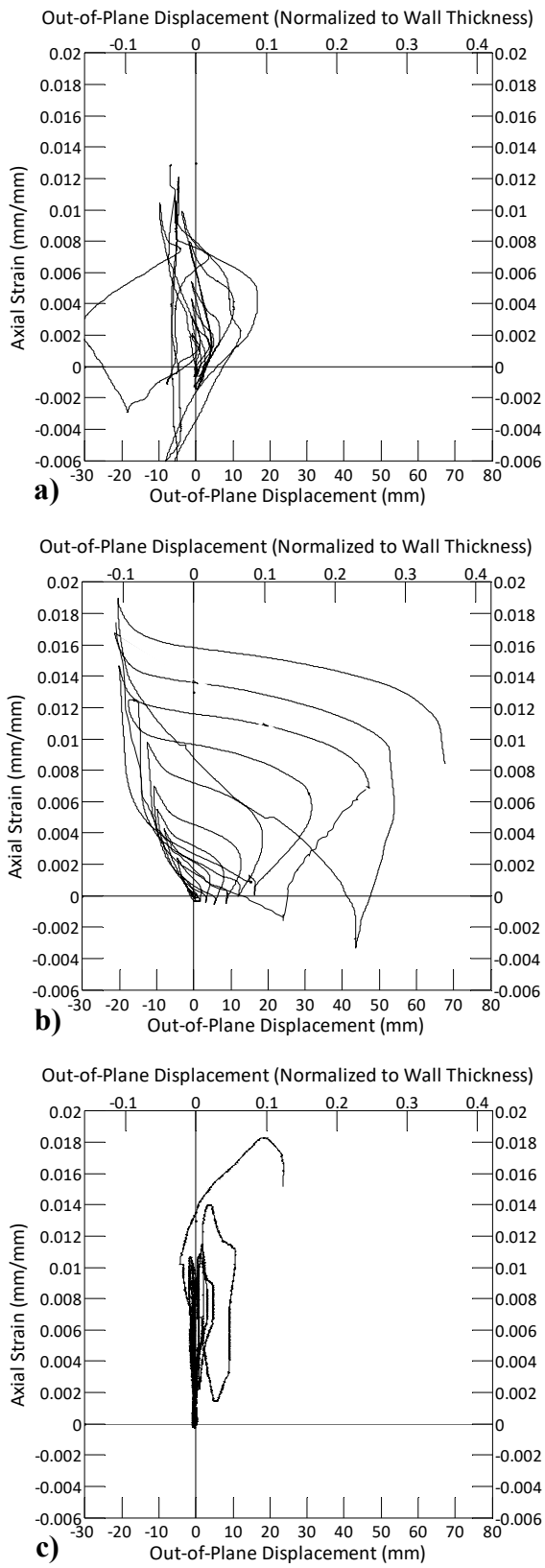

Figure 8: Ave end zone strain vs. out-of-plane displ.: a) W6, b) W7, and c) W8.

Figure 8 provides a visual comparison of the axial strain versus out-of-plane displacement relationships of specimens W6, W7, and W8. Only specimen W7 experienced significant out-of-plane displacements, whereas specimens W6 and W8 experienced relatively small out-of-plane displacements. Several factors appeared to influence the occurrence and non-occurrence of out-of-plane displacements among the specimens.

The large sliding displacements experienced by the unrestrained specimen W6 created a tendency for the reinforcing bars crossing the primary sliding plane, located at the base of the wall, to rotate and deform in the plane of the wall rather than out-of-plane; this greatly reduced the tendency of developing significant out-of-plane rotations and displacements. The low compression loading at the web end zone of specimen W6 failed to fully close the open flexural cracks over its height. This created a relatively rough crack surface compared to specimen W7, which had a symmetric loading protocol. It is believed this rough surface partially reduced out-of-plane rotations relative to a smooth crack surface.

The flanged boundary elements had clear effect on the out-of-plane response of the end zones. The increased lateral strength and stiffness prevented both Class B and C instability mechanisms from initializing. However, at high ductility levels, Class A instability still had significant affect in the form of vertical bar buckling following toe-crushing. The largest out-of-plane displacements of the web end zone of specimen W7 initially occurred at low levels of axial tensile strain, i.e. approximately 0.002, but progressively grew with increasing levels of tensile strain until the occurrence of face shell spalling and toe crushing. This was because the low applied axial stress permitted the strains to increase steadily in the same ratcheting-like fashion that affected specimen W6, although to a somewhat lesser extent. Likewise, the residual out-of-plane displacement corresponding to the point of maximum compressive strain also increased with each load cycle as the crack closure mechanism was initiated at progressively increasing out-of-plane displacement.

KEY FINDINGS

The flanged boundary elements of T-shaped RMSWs significantly improve the ultimate strength of the RMSW during loading toward the web end zone, but do not significantly increase the strength during loading toward the flanged end zone. Furthermore, it comparison between the T-shaped specimen W7 compared to the rectangular specimen W8 indicates more rapid strength degradation, decreased ductility, and lower residual strength during loading toward the web end zone of a T-shaped wall versus a rectangular wall.

The lengthened moment-arm between the compression stress block and the outermost vertical reinforcing bars increases the tensile strain in the vertical reinforcement at the web end zone relative to a rectangular RMSW end zone subjected to an equivalent lateral displacement demand. This in-turn indicates a higher vulnerability toward out-of-plane instability for the web end zone of a T-shaped wall as compared to a rectangular wall due to the close positive correlation between increasing tensile strains and out-of-plane displacements of an end zone

(Robazza et al. 2015b). On the opposite, flanged end zone of a T-shaped wall clearly has a higher resistance toward out-of-plane instability due to its greater lateral stiffness; however, as significant flexural cracks develop at the flanged end zone, this support degrades as the lateral stiffness of the flanged end zone transforms from the gross masonry cross-section to only that of the vertical reinforcing bars spanning the crack. Comparing specimens W6, W7, and W8 indicates that after flexural cracking of the flanged end zone occurs, a T-shaped wall may indeed actually be more susceptible to out-of-plane instability due to the increased axial tensile strains.

CONCLUSIONS

Compared to rectangular RMSWs, RMSWs with flanged boundary elements were found to possess higher strength during loading toward the web end zone, but not during loading toward the flanged end zone. Moreover, ductility was found to be significantly lower for loading toward the web end zone, with similar residual strength compared to rectangular RMSWs. Resistance toward out-of-plane instability was found to be higher for T-shaped RMSWs at low ductility levels, however, as cracking became more significant, T-shaped RMSWs become more susceptible to out-of-plane instability due to higher strains developing at the web end zone.

ACKNOWLEDGEMENTS

The project was sponsored by the Natural Sciences and Engineering Research Council of Canada (NSERC) through a Collaborative Research and Development Grant, the Canadian Concrete Masonry Producers Association, and the Masonry Institute of British Columbia. The first author acknowledges the support provided by the NSERC Industrial Postgraduate Scholarship program.

REFERENCES

[1] Canadian Standards Association (2004a). CSA A165-04: CSA Standards on concrete masonry units. CSA, Mississauga, ON, Canada.

[2] Canadian Standards Association (2004b). CSA, A179-04: CSA Mortar and grout for unit masonry. CSA, Mississauga, ON, Canada.

[3] Canadian Standards Association (2004c). CSA, G301.18-M92: Billet-steel bars for concrete reinforcement. CSA, Mississauga, ON, Canada.

[4] He L. and Priestley M. J. N. (1992). “Seismic Behavior of Flanged Masonry Shear Walls.” Research Report No. 4.1-2 - San Diego: Department of Applied Mechanics of Engineering Sciences, University of California, San Diego, CA, USA, p. 97-106.

[5] Paulay, T., and Priestley, M. (1992). “Seismic design of reinforced concrete and masonry buildings.” Wiley, New York, p. 397-408.

[6] Robazza, B.R., Brzev, S., Elwood, K.J., Anderson, D.L., Yang, T.Y. (2015a). “A study on the out-of-plane stability of ductile reinforced masonry shear walls subjected to in-plane reversed cyclic loading.” Proceedings of the 12th NAMC, Denver, CO, USA.

[7] Robazza, B.R., Brzev, S., Elwood, K.J., Anderson, D.L., Yang, T.Y. (2015b). “Effect of In-Plane Reversed-Cyclic Loading on the Out-of-Plane Stability of Reinforced Masonry Shear Walls.” Proceedings of the 11th CCEE, Victoria, BC, Canada.

[8] Shedid, M., Drysdale, R., and El-Dakhakhni, W. (2008). "Behavior of Fully Grouted Reinforced Concrete Masonry Shear Walls Failing in Flexure: Experimental Results." J. Struct. Eng., 10.1061/(ASCE)0733-9445(2008)134:11(1754), p.1754-1767.